Polymer 99 (2016) 97–104

Contents lists available at ScienceDirect

Polymer

journal homepage: www.elsevier.com/locate/polymer

Quantitative understanding of two distinct melting kinetics of an isothermally crystallized poly(ether ether ketone)

Yoshitomo Furushima [a, d, e, *], Akihiko Toda [b], Vincent Rousseaux [c], Christian Bailly [c], Evgeny Zhuravlev [d, e], Christoph Schick [d, e]

[a] Materials Characterization Laboratories, Toray Research Center Inc., 3-7, Sonoyama 3-chome, Otsu, Shiga 520-8567, Japan
[b] Graduate School of Integrated Arts and Sciences, Hiroshima University, Higashi-Hiroshima 739-8521, Japan
[c] Institute of Condensed Matter and Nanosciences, Universite Catholique de Louvain, 1348 Louvain-la-Neuve, Belgium
[d] Institute of Physics, University of Rostock, Albert-Einstein-Str. 23–24, 18059 Rostock, Germany
[e] Competence Centre CALOR, Faculty of Interdisciplinary Research, University of Rostock, Albert-Einstein-Str. 25, 18059 Rostock, Germany

ARTICLE INFO

Article history:
Received 26 May 2016
Received in revised form
29 June 2016
Accepted 1 July 2016
Available online 2 July 2016

Keywords:
Secondary nucleation
Multiple melting kinetics
Zero-entropy-production melting

ABSTRACT

The multiple melting peaks of isothermally crystallized poly(ether ether ketone) were investigated by fast-scanning chip calorimetry over a wide range of heating rates from 500 to 60,000 K s^{-1}. The analysis of heating rate dependence of melting temperatures revealed that there are two crystal populations with distinct melting kinetics for the samples prepared at different crystallization temperatures, 170 °C ≤ T_{iso} ≤ 270 °C. For each T_{iso}, the two melting temperatures of the metastable crystals without prior reorganization or superheating (i.e. zero-entropy-production melting temperatures) were constantly 20 K and 30 K, respectively, higher than T_{iso}. We first discuss this behavior quantitatively based on the Lauritzen-Hoffman nucleation approach. Finally we conclude that these increases in temperature are linked to the number of stems which construct the secondary surface nuclei. The existence of two crystal populations can be caused by differences in the stability of the crystal or "local" differences in the free energy of the surrounding melt.

© 2016 Elsevier Ltd. All rights reserved.

1. Introduction

Multiple melting behavior observed by differential scanning calorimetry (DSC) is well-known for many isothermally crystallized polymers. Marand et al. reported multiple melting of bisphenol-A polycarbonate, poly (arylene ether ether ketone), and ethylene/1-octane copolymers in conventional DSC curves, depending on the heating rate [1–3]. Such behavior could not be explained by a simple mechanism of melting-reorganization-remelting during heating. They concluded that two different crystals exist for these polymers. However, it is also said that reorganization during heating is not fully suppressed due to the slow-heating rate of conventional DSC.

A fast-scanning chip calorimetry (FSC) method developed by Schick et al. [4–10] succeeds in the kinetic study of crystallization/melting of semi-crystalline polymers at controlled scanning rates up to 100,000 K s^{-1} [11–21]. In a previous FSC study, the authors reported two crystal populations with different melting kinetics for isothermally crystallized polyamide 6 (PA 6) by suppressing the reorganization upon heating [13]. However, the attribution of the two crystals in PA 6 is still an open question due to the structural complexity of PA 6. Four possible assignments were considered:

(i) Crystals grown during primary and secondary crystallization. This assignment is similar to the one proposed in Marand et al. [1–3].
(ii) Crystals nucleated and grown in the bulk or nucleated at the surface/substrate [22].
(iii) Crystals which are subjected to different local stress originating from heterogeneities in interlamellar regions. Melnikov et al. assigned the double endotherm on the FSC curves for poly(trimethylene terephthalate) (PTT) in this a way, using an in-situ combination of synchrotron nano-focus X-ray scattering and nanocalorimetry [23]. The first melting is assigned to melting of the crystals confined in the smallest amorphous interlamellar regions, which can explain the negative stresses imposed on these crystals.

* Corresponding author. Materials Characterization Laboratories, Toray Research Center Inc., 3-7, Sonoyama 3-chome, Otsu, Shiga 520-8567, Japan.
E-mail address: furu1furu2furu3@gmail.com (Y. Furushima).

http://dx.doi.org/10.1016/j.polymer.2016.07.005
0032-3861/© 2016 Elsevier Ltd. All rights reserved.

(iv) The crystal/mesophase polymorphism in PA 6 [24–31]. It has been found that solidification at temperatures above about 150 °C leads to formation of monoclinic alpha-crystals, while solidification at lower temperature is connected with formation of a pseudohexagonal mesophase.

On the other hand, Schick et al. failed to find evidence for the formation of multimodal distributions of crystals which show multiple melting behaviors with substantially different stabilities for isothermal crystallization of poly(ethylene terephthalate) (PET) and isotactic polystyrene (iPS) [32–34]. This lack of evidence stems from the difficulty in exclusively investigating the melting of the originally formed crystals and the multiple melting peaks were attributed to melting-recrystallization-remelting processes in those polymers at slow heating.

In this study, the FSC experiments for poly(ether ether ketone) (PEEK) were carried out over a wide range of heating rate from 500 to 60,000 K s^{-1}. PEEK is one of the highest performance thermoplastics. Due to the advantageous thermal and mechanical properties [35], PEEK and its composites are widely used and the thermal properties of PEEK are well studied. It is known that isothermally crystallized PEEK shows double melting on conventional DSC curves [36–42]. FSC measurements were also reported for isothermally crystallized PEEK at a heating rate up to 2000 K s^{-1} [43,44]. The double melting peaks seem to reduce to a single peak at heating rate of 2000 K s^{-1} [43]. However, even at this heating rate, an endothermic shoulder due to the melting of reorganized crystals still remains. This means the reorganization during heating is not fully suppressed at a heating rate of 2000 K s^{-1}. This is in agreement with the PA 6 data, where the critical heating rate to suppress the reorganization is up to 50 times higher than the critical cooling rate to yield complete vitrification [13]. Therefore the kinetics of reorganization must be carefully considered for the understanding of multiple melting behavior. In addition, SAXS experiments suggest that a gradient of crystal perfection may exist along the lamellar thickness direction for isothermally crystallized PEEK [44]. This result may be related to the observation of multiple melting peaks. Note that polymorphism is not reported for PEEK. Hence the interpretation of FSC data could be simpler than that of PA 6. Taking into account these prior investigations, it is worth studying the heating rate dependence of FSC measurements over a wide range of heating rates to clarify the precise melting kinetics of PEEK. Another purpose of this study is to clarify the relation between crystallization temperature, melting temperature, and crystal structure. It is known that some semi-crystalline polymers including PEEK show the following relation between the melting peak temperature, T_m, and the crystallization temperature, T_{iso}; $T_m = T_{iso} + \delta T$ with a constant δT [13,16,41,42]. Quantitative consideration of this issue is discussed for the first time in the present study, based on the Lauritzen-Hoffman nucleation approach. We try to obtain a general insight on crystal structure from this thermodynamic model.

2. Experimental

An amorphous PEEK film (Stabar K200) from Imperial Chemical Industries (ICI, UK) was investigated in this study. Molecular weight, M_w, was 95,000–120,000 g mol^{-1}. Note that the original morphology of the sample was destroyed because of pre-melting and isothermal annealing before the measurements, as shown in Fig. 1.

FSC measurements were carried out using a Mettler Toledo Flash DSC 1 [6–8] and a home build FSC with the XI390 chip calorimeter (XEN-39390). Details of the second device and the data treatment have been reported elsewhere [9,10]. In this study, one sample was placed directly on the sensor and pre-melted at 400 °C for 0.1 s to establish a good thermal contact between the sample and the sensor. All experiments with the XI390 sensor were performed with this sample. Due to the short residence time at high temperature degradation was not observed. The curve labeled (a) in Fig. 1 shows the temperature-time program of the XI390 chip calorimeter measurements, showing that the temperatures of isothermal crystallization, T_{iso}, being between 170 and 270 °C, were approached by cooling the melt from 400 °C at a rate of 50,000 K s^{-1}; the crystallization time was 1800 s, with the exception of 900 s for crystallization at 270 °C. After completion of crystallization, the samples were cooled down to −173 °C, which is far below the glass transition temperature, T_g of 146 °C [45] at a cooling rate of 50,000 K s^{-1}. Finally, the samples were reheated at different rates between 500 and 60,000 K s^{-1}, for analysis of the metastability of the crystals formed at the various temperatures. The critical cooling rate to quench crystallization upon continuous cooling to below T_g has been reported to be 2 K s^{-1} for PEEK [39]. The cooling rate adopted in this study is faster than the critical cooling rate. Hence, crystallization only proceeds during the subsequent isothermal annealing. In addition, it is reported that the half time of isothermal crystallization of PEEK is below 10 s for T_{iso} ranging from 150 to 270 °C [46]. In addition, at T_{iso} of 300 °C, the crystallinity saturates below 1000 s [46]. Consequently, we infer that primary crystallization is completed within the annealing time of 900 or 1800 s used in our study. A sample mass of 10 ng was estimated from the change in heat capacity at the glass transition temperature for an amorphous sample (quenched from the molten state at a rate of 50,000 K s^{-1}). No change in the sample mass before or after the measurements was detected. The accuracy of the temperature was experimentally confirmed by an indium standard placed beside the sample on the chip sensor.

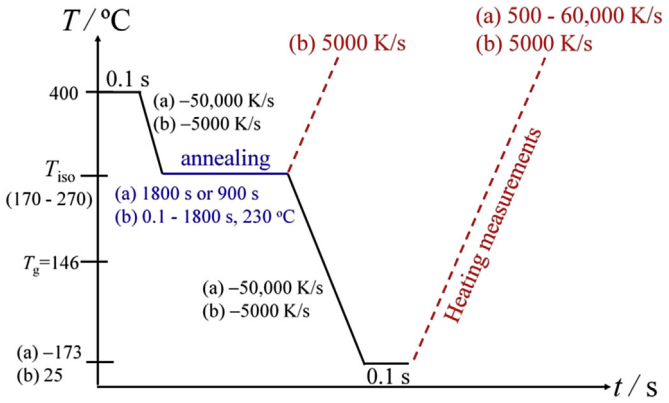

Fig. 1. Temperature-time program of (a) XI390 chip calorimeter and (b) Flash DSC 1.

For a fixed heating rate of 5000 K s^{-1} additional FSC measurements were carried out using a Flash DSC 1 (Mettler-Toledo, Switzerland). The temperature-time program of the Flash DSC 1 measurements is labeled (b) in Fig. 1. The measurements were carried out for the isothermally crystallized samples with different annealing times at 230 °C. Two kinds of measurements were performed to confirm the crystallization proceeds only during annealing. Namely we performed additional measurements where the samples were heated directly from T_{iso} to the melt. A sample mass of 75 ng was estimated from the change in heat capacity at the glass transition temperature for the amorphous sample (quenched from the molten state at a rate of 5000 K s^{-1}). The sample mass did not change during the course of the measurements. The accuracy of the temperature was experimentally confirmed by an indium standard placed onto the sample.

3. Results

3.1. Heating rate dependence of melting

Fig. 2 shows FSC curves of isothermally crystalized PEEK at heating rates ranging from 500 to 60,000 K s^{-1}. As shown in Fig. 2(a), two endothermic peaks at 230 °C and 300 °C, marked peaks II and III, were observed at a heating rate of 500 K s^{-1}. Peak II shifts to higher temperature with increasing heating rate due to superheating. On the other hand, peak III gradually shifts to lower temperature and the corresponding heat of fusion decreases with increasing heating rate. This result strongly suggests that peak III is due to the melting of reorganized crystals, namely the reorganization during heating is increasingly suppressed with increasing heating rate. As for the case of T_{iso} = 190 °C, peak III disappears at a heating rate above 20,000 K s^{-1}. Comparing curves at the same heating rate for different T_{iso}, peak II shifts to higher temperature with increasing T_{iso}. Moreover, peak III disappears at a lower heating rate as T_{iso} increases (i.e. 10,000 K s^{-1} for T_{iso} = 210 °C, 5000 K s^{-1} for T_{iso} = 230 °C, 2000 K s^{-1} for T_{iso} = 250 °C, and 2000 K s^{-1} for T_{iso} = 270 °C).

It is noteworthy to mention that at heating rates above 20,000 K s^{-1}, an additional endothermic shoulder, marked as peak I, appears below the peak temperature. Peak I also shifts to higher temperature with increasing heating rate. As compared to peak II, peak I shifts only by a small amount with heating rate. Such kind of additional peak observed at fast heating rate was first reported for isothermally crystallized PA 6 [13]. The difference between PA 6 and PEEK is that the additional endothermic peak of PA 6 shows up at a higher temperature than the main endothermic peak.

Here, since the sample mass and thickness are sufficiently small, the broad, heating rate dependent, melting behavior of the polymer crystals is not due to thermal lag [14–17]. According to these references, the influence of thermal lag is negligible for the sample mass of 10 ng used in the present study with the XI390 chip calorimeter. Furthermore, a previous study also shows that the temperature-shift due to thermal lag at fast heating is only a few Kelvin for the thin samples used [12].

3.2. Crystallization time dependence of melting

Fig. 3 shows the crystallization time dependence of FSC curves for T_{iso} = 230 °C. The melting peak II stays at a fixed temperature from the early stage of crystallization, namely for isolated lamellar crystals without constraints the melt. Time-resolved small-angle X-ray scattering (SAXS) results also show that during the isothermal crystallization, the average lamellar thickness remains almost constant with increasing annealing time [47]. In contrast, the lower side of the melting peak seems to shift gradually to higher temperature with increasing annealing time. This shift can be due to a decrease of the entropy of the melt, as it becomes more tightly constrained by the progress of the secondary crystallization.

To confirm that no crystallization occurred during the cooling process, we carried out an additional measurement in which the sample was heated directly from the T_{iso} to the molten state. As shown in Fig. 4, both FSC traces were fully consistent in the melting region independent of annealing time. These results indicate that crystallization upon quenching from T_{iso} to 25 °C and re-heating to T_{iso} is fully suppressed (i.e., crystallization proceeds only during the isothermal process and for slow heating rates upon further heating). Note that the curve at the time of 1800 s in Fig. 3 and the curve at a rate of 5000 K s^{-1} in Fig. 2(c) are obtained for almost identical sample preparations. The melting peak in Fig. 3 is higher than that in Fig. 2(c) due to the larger sample mass for the measurements in the Flash DSC 1. The relationship between sample shape and/or contact surface area of the sample, sample mass, and double melting kinetics awaits a future investigation.

For reference, the Kolmogorov-Johnson-Mehl-Avrami equation [48,49] was applied to fit the enthalpy of melting as a function of annealing time. A crystallization half-time, $t_{1/2}$, of 1.47 s and Avrami coefficient, n, of 3 were estimated for isothermally crystallized PEEK at T_{iso} of 230 °C. The $t_{1/2}$ in the present study is about 1 s faster than the value reported in the previous study [43] probably due to the different PEEK grade used.

4. Discussion

4.1. Two melting kinetics

Fig. 5 summarizes the heating rate dependence of melting peak temperatures, T_m. Note that both analytical peak separation by two Gaussian functions and visual confirmation were carried out in order to evaluate the T_m from overlapped peaks. This estimation includes an error of approximately ±5 K. Peaks I and II increase with increasing heating rate for each T_{iso}. Furthermore, comparing the same heating rates, it seems that the $T_m - T_{iso}$ of peaks I and II decreases with increasing T_{iso}. On the other hand, peak III decreases with increasing heating rate because of the suppression of reorganization during heating. Peak III is attributed to the melting of reorganized crystals. In this study we give the same indices I, II or III to the crystals as to the corresponding endotherms.

As shown in Fig. 5, peak I appears at fast heating rates after peak III disappears. This can be explained that if we assume the reorganization of crystal II is only activated by the presence of the molten polymer chains formerly comprising crystal I. In this situation, first at low heating rates below the critical heating rate to suppress the reorganization, crystal I melts at lower temperature, and at the same time, crystal II starts to reorganize to become crystal III, which has higher melting temperature.

The critical heating rate to suppress the reorganization (i.e. the heating rate which peak III completely disappears from the FSC curve) is shown in Fig. 6. The critical heating rate to avoid reorganization tends to decrease as increasing T_{iso}. The suppression of reorganization during slow heating at high T_{iso} suggests the formation of more stable crystals with increasing T_{iso} and finally a decreasing critical heating rate. The same behavior was observed for PA 6 and isotactic polypropylene (iPP) [13,50]. For PEEK, the critical heating rate to suppress reorganization is more than 1000 times higher than the critical cooling rate to avoid crystallization upon continuous cooling to below T_g.

Next, we consider the superheating kinetics for crystals I and II. The heating rate dependence of the melting temperatures of superheated crystals was originally suggested by Schawe et al. and was extended to general cases by Toda et al. [51,52] as follows:

$$T_m = T_{ZEP} + A\beta^z \quad \text{with } 0 < z \leq 0.5 \tag{1}$$

where T_m is the peak melting temperature, T_{ZEP} is the zero-entropy-production (ZEP) melting temperature, A is a constant, β is the heating rate, and z is an exponent. The ZEP melting refers to the melting of a metastable crystal at its stability limit, i.e., without prior reorganization or superheating. Equation (1) suggests that T_{ZEP} can be obtained by extrapolating T_m to zero heating rate. Fig. 7 show the relationship between $T_m - T_{iso}$ and heating rate with power (β^z) for peaks I and II. The best linear fits with z-values of 0.45 are also shown in Fig. 7. Lower z-values ($z < 0.5$) indicate melting kinetics with a high activation barrier. The melting temperature increases with the heating rate because of superheating. Here, superheating describes the melting of a crystal at a temperature above that expected from equilibrium conditions. As color-coded

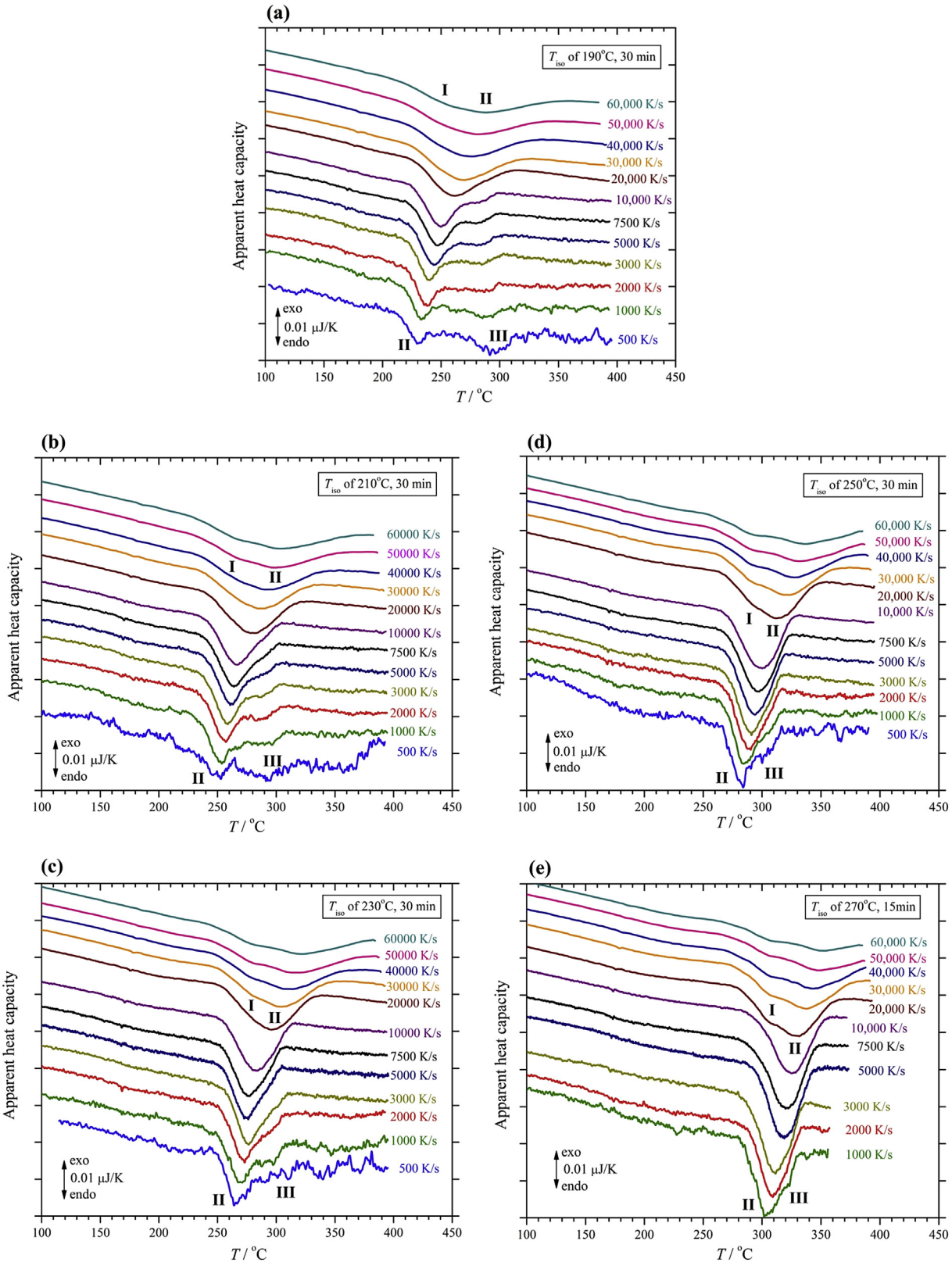

Fig. 2. Heating-rate dependence of FSC curves of isothermally crystalized PEEK: (a) T_{iso} = 190 °C, annealing time of 30 min, (b) T_{iso} = 210 °C, annealing time of 30 min, (c) T_{iso} = 230 °C, annealing time of 30 min, (d) T_{iso} = 250 °C, annealing time of 30 min, and (e) T_{iso} = 270 °C, annealing time of 15 min.

for each T_{iso} in Fig. 7, extrapolation lines of peaks I and II with different slopes yield intersects, which are independent of T_{iso} within the ±5 K experimental error on T_{ZEP}. These results strongly suggest the existence of two crystal populations with distinct melting kinetics for isothermally crystallized PEEK. As discussed below, the y-intersect of the extrapolations for both peaks I and II

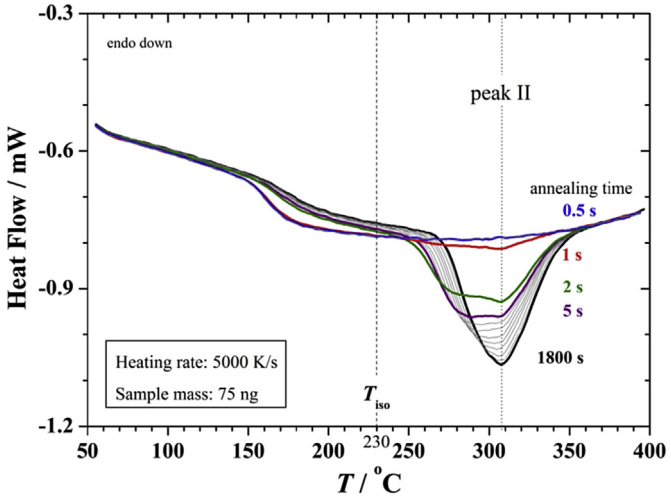

Fig. 3. FSC curves collected at a heating rate of 5000 K s^{-1}. The samples were prepared at T_{iso} of 230 °C for times indicated. FSC curves were obtained with Flash DSC 1. The sample mass was 75 ng.

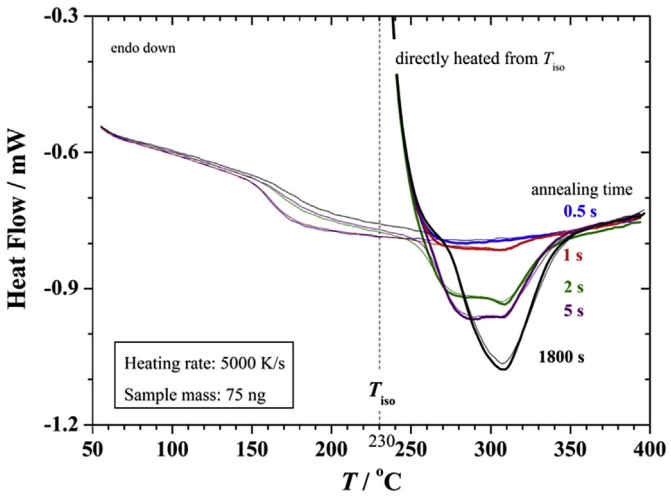

Fig. 4. FSC curves for PEEK at a heating rate of 5000 K s^{-1}. The samples were crystallized at 230 °C for times indicated. Thin lines are the same FSC curves as showed in Fig. 3. Thick lines are the FSC curves directly heated from T_{iso}. FSC curves were obtained with Flash DSC 1.

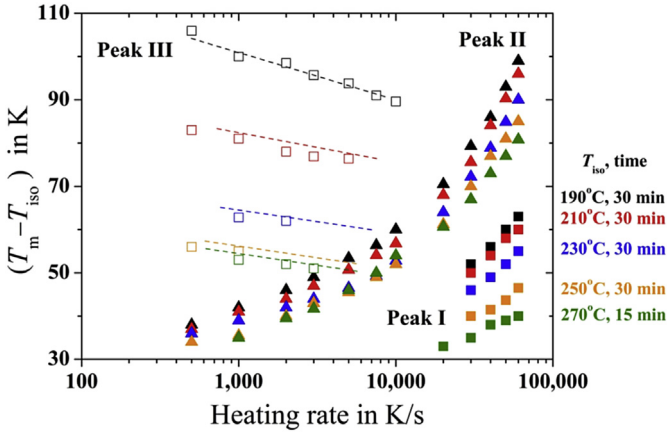

Fig. 5. Heating rate dependence of peak melting temperature of isothermally crystallized PEEK at annealing temperatures ranged from 190 to 270 °C.

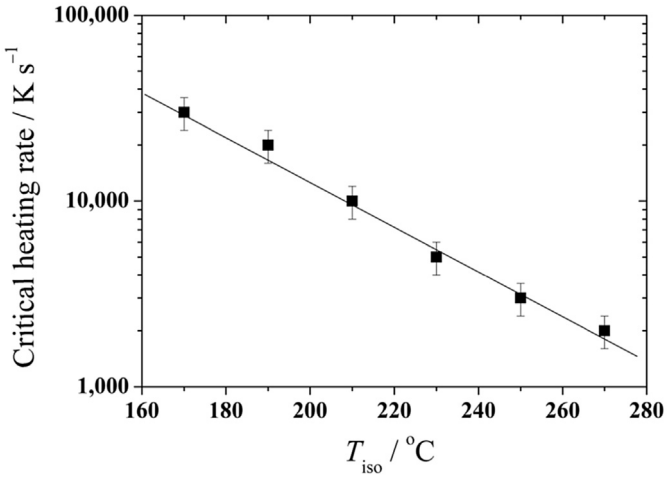

Fig. 6. Isothermal temperature dependence of critical heating rate for PEEK at annealing time of 30 min (including an approximate error of ±20%). The line is a guide to the eyes only.

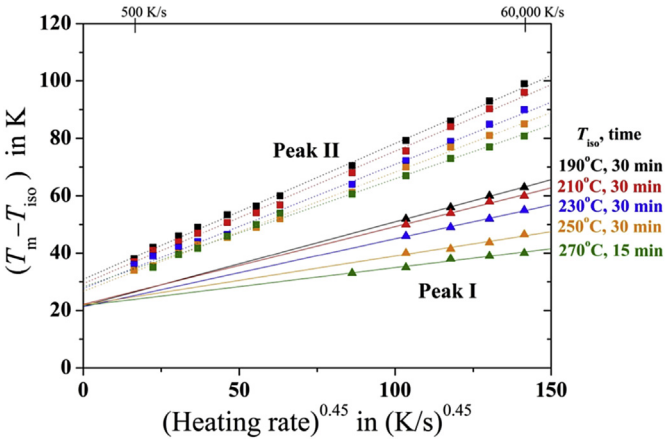

Fig. 7. Melting peak temperatures against heating rate with a power of 0.45 for isothermally crystallized PEEK.

are independent of T_{iso}. Real time small angle X-ray scattering indeed supports the existence of two crystals for isothermal crystallized PEEK [46].

According to Ivanov et al., the first melting peak (peak I) is assigned to the melting of crystals confined in the smallest amorphous gaps. The lower melting temperature can be explained by negative stresses imposed on these crystals [23]. Wurm et al. also discussed the surface of a polymer crystal after long isothermal crystallization [53,54]. A fraction of a given polymer chain may be part of a crystalline lamella and another fraction part of the melt. Therefore it is not possible to attach more segments to one or the other crystal due to geometric restrictions. The same may happen if the chain is part of the same crystal or because of entanglements in the amorphous regions. One can therefore argue that changes in T_{ZEP} of two crystals reflect differences in the "local" equilibrium between the melting crystal and the surrounding melt. This can be caused by differences in the stability of the crystal or "local" differences in the free energy of the surrounding melt.

4.2. Zero-entropy-production melting

ZEP melting temperatures of peaks I and II were obtained by

extrapolating the plots to a heating rate of zero in Fig. 7. Extrapolation lines of peaks I and II with different slopes yields two common intersects for the different T_{iso}. Fig. 8 shows the plots of T_{ZEP} against T_{iso} for isothermally crystallized PEEK. The ZEP melting temperature increases with increasing T_{iso}, suggesting thicker lamellae with increasing T_{iso}. The linear relationship between T_{ZEP} and T_{iso} (i.e., the Hoffman–Weeks equation [55]) is expressed as follows:

$$T_{ZEP} = \frac{1}{\gamma} T_{iso} + \left(1 - \frac{1}{\gamma}\right) T_m^0 \tag{2}$$

where γ is a constant representing the lamella thickening factor and T_m^0 is the equilibrium melting temperature. Here the lamella thickening factor is defined by the ratio between the lamellar thickness at the time of melting, d_c, and the critical lamellar thickness, d_c^* ($\gamma \equiv d_c/d_c^*$). Hoffman–Weeks plots are normally used to determine the equilibrium melting temperature, T_m^0, which is defined as the melting temperature of a perfect crystal formed by an infinite stack of extended chains. T_m^0 is then estimated from the intersection between the linear extrapolation of the plot in Fig. 8 and the line with slope 1, in black in the figure (i.e., $T_{iso} = T_{ZEP}$). The T_{ZEP} of the melting onset temperature seems equal to T_{iso} which means the lamellar thickness remains at the critical value and crystal growth does not proceed during annealing. However, within the ±5 K experimental uncertainty on T_{ZEP} the data for peaks I and II show a trend parallel to the black line (i.e. $\gamma = 1$) as shown in the following relationship between the peak temperature, T_{ZEP}, and the crystallization temperature, T_{iso};

$$T_{ZEP} = T_{iso} + \delta T \tag{3}$$

with a constant δT. Marand et al. theoretically discussed linear and non-linear Hoffman-Weeks extrapolations taking into account a thickness increment above the minimum lamellar thickness [56,57]. However, even in the case of $\gamma = 1$, their modified Hoffman-Weeks extrapolations cannot explain the present result of Eq. (3). Interestingly, a similar behavior was already reported for some polymers such as PA 6, iPP, PEEK, poly(butylene terephthalate) (PBT), poly(ε-caprolactone) (PCL), poly(butylene succinate) (PBS), and poly(vinylidene fluoride) (PVDF) [13,16,41,42,58–62].

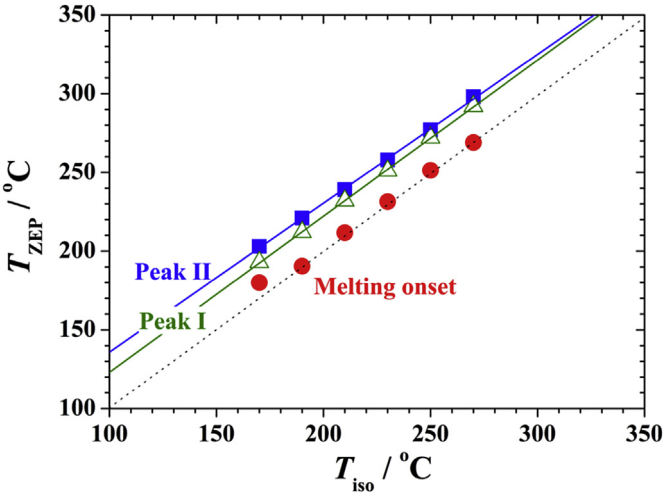

Fig. 8. Plots of T_{ZEP} against T_{iso} (Hoffman–Weeks plot) for isothermally crystallized PEEK. Open-triangle, filled-square, and filled-circle represent the results for peaks I, II, and onset, respectively. The black dotted line represents $T_{ZEP} = T_{iso}$.

4.3. Quantitative understanding of $T_{ZEP} = T_{iso} + \delta T$

The difference in chemical potential between a bulk crystal and the bulk melt is given as,

$$\Delta\mu^0(T) \cong \Delta h_f \frac{T_m^0 - T}{T_m^0} \tag{4}$$

with T_m^0 the equilibrium melting point of an extended-chain infinite-sized crystal and Δh_f the heat of fusion of an extended-chain infinite-sized crystal.

Basically first-order phase transition, such as crystallization, needs a finite chemical potential gap between the melt and the crystal to proceed. The Lauritzen-Hoffman nucleation model of polymer crystallization [55] assumes a constant excess of lamellar thickness, δd_c, from the critical minimum thickness, d_c^*,

$$d_c = d_c^* + \delta d_c, \tag{5}$$

for crystallization to proceed, especially from dilute solution. Here, for the crystallization of PEEK from the melt over the examined range of T_{iso}, the experimentally obtained relationship of Eq. (3) seems to suggest a constant chemical potential gap as in Eq. (4), instead of a constant increment of lamellar thickness as in Eq. (5). The following is a possible explanation for this behavior.

The ZEP melting temperature, T_{ZEP}, of the lamellar crystal of thickness d_c is given by the balance of $2\sigma_e - d_c\Delta\mu^0(T) \cong 0$, as follows;

$$T_{ZEP} = T_m^0 \left(1 - \frac{2\sigma_e}{\Delta h_f} \frac{1}{d_c}\right) \tag{6}$$

where σ_e is fold surface free energy.

From Eqs. (3), (4) and (6), lamellar thickness can be expressed as follows;

$$d_c = \frac{2\sigma_e}{\Delta h_f} \frac{T_m^0}{T_m^0 - T_{ZEP}} = \frac{2\sigma_e}{\Delta h_f} \frac{T_m^0}{\left(T_m^0 - T_{iso}\right) - \delta T} = \frac{2\sigma_e}{\Delta\mu^0(T_{iso}) - \Delta h_f \frac{\delta T}{T_m^0}} \tag{7}$$

In terms of secondary surface nucleation at T_{iso}, the Gibbs free energy difference between a surface nucleus and the bulk melt is given as follows;

$$\Delta G = -\Delta\mu^0(T_{iso})(nabd_c) + 2\sigma_e(nab) + 2\sigma(bd_c) \tag{8}$$

where the secondary surface nucleus is of thickness d_c and number of stems is n. The secondary surface nucleus is of lateral width a and thickness b (see (a) in Fig. 9).

A stable nucleus which can continue to grow should have $\Delta G < 0$. As shown in (b) in Fig. 9, the border is given by $\Delta G^{**} = 0$ with d_c^{**} and n^{**}. Hence Eq. (8) can be rewritten as;

$$d_c^{**} = \frac{2\sigma_e (n^{**}a)}{\Delta\mu^0(T_{iso})(n^{**}a) - 2\sigma} = \frac{2\sigma_e}{\Delta\mu^0(T_{iso}) - \frac{2\sigma}{n^{**}a}} \tag{9}$$

Comparing both Eqs. (7) and (9), one can notice that the experimental result of Eq. (3) can be explained if the lamellar thickness is controlled by (in other words, does not increase beyond) this thickness d_c^{**} of stable nuclei while the number of stem n^{**} is not dependent on T_{iso}, namely

$$n^{**}a = \frac{2\sigma}{\Delta h_f} \frac{T_m^0}{\delta T} \text{(indep. of } T_{iso}) \tag{10}$$

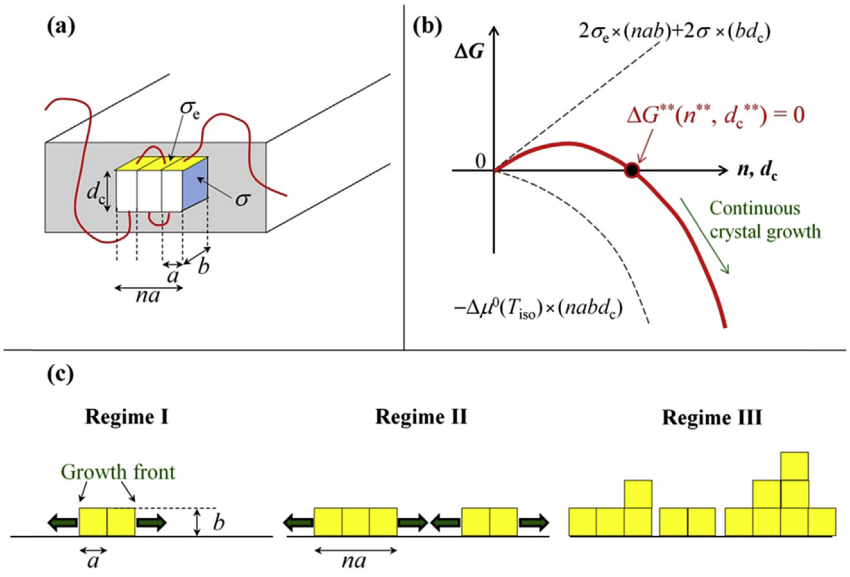

Fig. 9. Schematic image of (a) crystal, (b) Gibbs free energy diagram of crystallization, and (c) Regime of crystallization.

This behavior of $n^{**}a$ independent of T_{iso} can be expected for Regime III growth (see (c) in Fig. 9), where the number of stems is strongly limited by frequent neighboring nucleation events at large supercooling. It is noted that the importance of the minimum size of a stable surface crystal at $\Delta G^{**} = 0$ has attracted attention in a recent work by Xu et al. [61] who discuss the physical meaning of the intersection between melting and crystallization lines.

It is now interesting to evaluate $n^{**}a$ of Eq. (10) to see whether n^{**} is a realistic number. In Eq. (10), according to Hoffman et al. [63,64], the following expression is approximately correct:

$$\frac{\sigma}{\Delta h_f} \sim 0.15(abc)^{1/3} \tag{11}$$

hence,

$$n^{**} \sim 0.3\left(\frac{bc}{a^2}\right)^{1/3}\frac{T_m^0}{\delta T} \sim 0.3\frac{T_m^0}{\delta T} \tag{12}$$

Here, according to the reference, the value (bc/a^2) is 0.98 [65,66]. Hence, for $\delta T = 20$ K (peak I) and $T_m^0 = 668$ K for PEEK [45], n^{**} can be calculated as ~10. In addition, for $\delta T = 30$ K (peak II), n^{**} becomes ~7.

A similar number of stems was obtained from a similar analysis of the melting behavior of PCL in Ref. [60]. In the case of PCL isothermally crystallized at T_{iso} between 30 and 40 °C for 1800 s, δT is 17 K, hence n^{**} can be estimated as 6. This indicates that under these conditions the number of stems is around 10 for linear polymers.

5. Conclusion

Two distinct crystal populations were confirmed for isothermally crystallized PEEK by means of fast heating calorimetric experiments. Zero-entropy-production melting temperatures, T_{ZEP}, of the two kinds of crystal were determined from the analysis of superheating. One can argue that changes in T_{ZEP} of two crystals reflect differences in the "local" equilibrium between the melting crystal and the surrounding melt. This can be caused by differences in the stability of the crystal or "local" differences in the free energy of the surrounding melt.

Furthermore, a linear relationship between T_{ZEP} and T_{iso} with $T_{ZEP} = T_{iso} + \delta T$ was observed for both crystals in a T_{iso} range from 170 to 270 °C. A similar behavior has been reported for polymers such as PA 6, iPP, PEEK, PBT, PCL, PBS, and PVDF [13,16,41,42,58–62]. In the present study, we quantitatively explain the observation for the first time, in the framework of the Lauritzen-Hoffman nucleation approach [55]. It is concluded that the observed constant δT depends on the number of stems of the secondary nuclei, which is likely strongly limited by frequent neighboring nucleation events at large supercooling. The number of stems of the two distinct crystal populations is calculated to be around 10, which is close to that obtained from a similar analysis of a PCL sample.

Acknowledgements

YF acknowledges Toray Research Center, Inc. for supporting his stay at University of Rostock.

References

[1] S. Sohn, A. Alizade, H. Marand, On the multiple melting behavior of bisphenol-A polycarbonate, Polymer 41 (2000) 8879–8886.
[2] A. Alizadeh, L. Richardson, J. Xu, S. McCartney, H. Marand, Y.W. Cheung, S. Chum, Influence of structural and topological constraints on the crystallization and melting behavior of polymers. 1. Ethylene/1-Octene copolymers, Macromolecules 32 (1999) 6221–6235.
[3] H. Marand, A. Alizadeh, R. Farmer, R. Desai, V. Velokov, Influence of structural and topological constraints on the crystallization and melting behavior of polymers. 2. Poly(arylene ether ether ketone), Macromolecules 33 (2000) 3392–3402.
[4] A.A. Minakov, C. Schick, Ultrafast thermal processing and nanocalorimetry at heating and cooling rates up to 1MK/s, Rev. Sci. Instrum. 78 (2007) 073902–073910.
[5] E. Zhuravlev, C. Schick, Fast scanning power compensated differential scanning nano-calorimeter: 1. The device, Thermochim. Acta 505 (2010) 1–13.
[6] V. Mathot, M. Pyda, T. Pijpers, G. Vanden Poel, E. van de Kerkhof, S. van Herwaarden, F. van Herwaarden, A. Leenaers, The Flash DSC 1, a power compensation twin-type, chip-based fast scanning calorimeter (FSC): first findings on polymers, Thermochim. Acta 522 (2011) 36–45.
[7] S. van Herwaarden, E. Iervolino, F. van Herwaarden, T. Wijffels, A. Leenaers, V. Mathot, Design, performance and analysis of thermal lag of the UFS1 twin-calorimeter chip for fast scanning calorimetry using the Mettler-Toledo Flash DSC 1, Thermochim. Acta 522 (2011) 46–52.
[8] E. Iervolino, A.W. van Herwaarden, F.G. van Herwaarden, E. van de Kerkhof, P.P.W. van Grinsven, A.C.H.I. Leenaers, V.B.F. Mathot, P.M. Sarro, Temperature calibration and electrical characterization of the differential scanning calorimeter chip UFS1 for the Mettler-Toledo Flash DSC 1, Thermochim. Acta 522

(2011) 53–59.
[9] E. Zhuravlev, C. Schick, Fast scanning power compensated differential scanning nano-calorimeter: 1. The device, Thermochim. Acta 50 (1–2) (2010) 1–13.
[10] E. Zhuravlev, C. Schick, Fast scanning power compensated differential scanning nano-calorimeter: 2. Heat Capacity analysis, Thermochim. Acta 50 (1–2) (2010) 14–21.
[11] A. Toda, R. Androsch, C. Schick, Insights into polymer crystallization and melting from fast scanning chip calorimetry, Polymer 91 (2016) 239–263.
[12] Y. Furushima, M. Nakada, M. Murakami, T. Yamane, A. Toda, C. Schick, Method for calculation of the lamellar thickness distribution of not-reorganized linear polyethylene using fast scanning calorimetry in heating, Macromolecules 48 (2015) 8831–8837.
[13] Y. Furushima, M. Nakada, K. Ishikiriyama, A. Toda, R. Androsch, E. Zhuravlev, C. Schick, Two crystal populations with different melting/reorganization kinetics of isothermally melt crystallized polyamide 6, J. Polym. Sci. B Polym. Phys. (2016) (in press).
[14] A. Toda, Heating rate dependence of melting peak temperature examined by DSC of heat flux type, J. Therm. Anal. Calorim. 123 (2016) 1795–1808.
[15] A. Toda, K. Taguchi, K. Nozaki, M. Konishi, Melting behaviors of polyethylene crystals: an application of fast-scan DSC, Polymer 55 (2014) 3186–3194.
[16] A. Toda, K. Taguchi, K. Sato, K. Nozaki, M. Maruyama, K. Tagashira, M. Konishi, Melting kinetics of it-polypropylene crystals over wide heating rates, J. Therm. Anal. Calorim. 113 (2013) 1231–1237.
[17] A. Toda, M. Konishi, An evaluation of thermal lags of fast-scan microchip DSC with polymer film samples, Thermochim. Acta 589 (2014) 262–269.
[18] R. Androsch, C. Schick, Crystal nucleation of polymers at high supercooling of the melt, Adv. Polym. Sci. (2016) 1–32.
[19] R.T. Tol, A.A. Minakov, S.A. Adamovsky, V.B.F. Mathot, C. Schick, Metastability of polymer crystallites formed at low temperature studied by ultra fast calorimetry, polyamide 6 confined in sub-micrometer droplets vs bulk PA6, Polymer 47 (2006) 2172–2178.
[20] A. Wurm, A. Herrmann, M. Cornelius, E. Zhuravlev, D. Pospiech, R. Nicula, C. Schick, Temperature dependency of nucleation efficiency of carbon nanotubes in PET and PBT, Macromol. Mater. Eng. 300 (2015) 637–649.
[21] E. Zhuravlev, J. Schmelzer, A.S. Abyzov, V.M. Fokin, R. Androsch, C. Schick, Experimental test of Tammann's nuclei development approach in crystallization of macromolecules, Cryst. Growth Des. 15 (2015) 786–798.
[22] A. Wurm, M. Ismail, B. Kretzschmar, D. Pospiech, C. Schick, Retarded crystallization in polyamide/layered silicates nanocomosites caused by an immobilized interphase, Macromolecules 43 (2010) 1480–1487.
[23] A.P. Melnikov, M. Rosenthal, A.I. Rodygin, D. Doblas, D.V. Anokhin, M. Burghammer, D.A. Ivanov, Re-exploring the double-melting behavior of semirigid-chain polymers with an in-situ combination of synchrotron nanofocus X-ray scattering and nanocalorimetry, Eur. Polym. J. (2016), http://dx.doi.org/10.1016/j.eurpolymj.2015.12.031 (in press).
[24] K.-H. Illers, H. Haberkorn, Schmelzverhalten, Struktur und Kristallinität von 6-polyamid, Macromol. Chem. 142 (1971) 31–67.
[25] M. Kyotani, S. Mitsuhashi, Studies on crystalline forms of Nylon 6. II. Crystallization from the melt, J. Polym. Sci. Part A 2 10 (1972) 1497–1508.
[26] V. Brucato, S. Piccarolo, G. Titomanlio, Crystallization kinetics in relation to polymer processing, Macromol. Chem. Macromol. Symp. 68 (1993) 245–255.
[27] G. Gurato, A. Fichera, F.Z. Grandi, R. Zannetti, P. Canal, Crystallinity and polymorphism of 6-polyamide, Macromol. Chem. 175 (1974) 953–975.
[28] D. Cavallo, L. Gardella, G.C. Alfonso, G. Portale, L. Balzano, R. Androsch, Effect of cooling rate on the crystal/mesophase polymorphism of polyamide 6, Colloid Polym. Sci. 289 (2011) 1073–1079.
[29] A. Ziabicki, Über die mesomorphe b-Form von Polycapronamid und ihre Umwandlung in die kristalline Form a, Kolloid-Zeitschrift Zeitschrift Polym. 167 (1959) 132–141.
[30] H. Hendus, K.H. Illers, P. Simak, Kristallisation von amorphem 6-polyamid im Glasüberg-angsbereich, Kolloid-Zeitschrift Zeitschrift Polym. 235 (1969) 1244–1246.
[31] W. Kozlowski, Kinetics of crystallization of polyamide 6 from the glassy state, J. Polym. Sci. Part C 38 (1972) 47–59.
[32] A.A. Minakov, D.A. Mordvintsev, C. Schick, Melting and reorganization of poly (ethylene terephthalate) on fast heating (1000 K/s), Polymer 45 (2004) 3755–3763.
[33] A.A. Minakov, D.A. Mordvintsev, C. Schick, Isothermal reorganization of poly(ethylene terephthalate) revealed by fast calorimetry (1000 K s−1; 5 ms), Faraday Discuss. 128 (2005) 261–270.
[34] A.A. Minakov, D.A. Mordvintsev, R. Tol, C. Schick, Melting and reorganization of the crystalline fraction and relaxation of the rigid amorphous fraction of isotactic polystyrene on fast heating (30,000 K/min), Thermochim. Acta 442 (2006) 25–30.
[35] D.P. Jones, D.C. Leach, D.R. Moore, Mechanical properties of poly(ether-ether-ketone) for engineering applications, Polymer 26 (1985) 1385–1393.
[36] S.Z.D. Cheng, B. Wunderlich, Heat capacities and entropies of liquid, high-melting-point polymers containing phenylene groups, J. Polym. Sci. B Polym. Phys. 24 (1986) 1755–1765.
[37] D.A. Ivanov, R. Legras, A.M. Jonas, Interdependencies between the evolution of amorphous and crystalline regions during isothermal cold crystallization of poly(ether–ether–ketone), Macromolecules 32 (1999) 1582–1592.
[38] C. Wei, M. Chen, F. Yu, Temperature modulated DSC and DSC studies on the origin of double melting peaks in poly(ether–ether–ketone), Polymer 44 (2003) 8185–8193.
[39] C.N. Velisaris, J.C. Seferis, Crystallization kinetics of polyetheretherketone (PEEK) matrices, Polym. Eng. Sci. 26 (1986) 1574–1581.
[40] D.J. Blundell, On the interpretation of multiple melting peaks in poly (ether ether ketone), Polymer 28 (1987) 2248–2251.
[41] Y. Lee, R.S. Porte, Double-Melting behavior of Poly(ether ether ketone), Macromolecules 20 (1987) 1336–1341.
[42] H.S. Chen, R.S. Porter, Melting behavior of poly(ether ether ketone) in its blends with poly (ether imide), J. Polym. Sci. B Polym. Phys. 31 (1993) 1845–1850.
[43] X. Tardif, B. Pigno, N. Boyard, J.W.P. Schmelzer, V. Sobotka, D. Delaunay, C. Schick, Experimental study of crystallization of PolyEtherEtherKetone (PEEK) over a large temperature range using a nano-calorimeter, Polym. Test. 36 (2014) 10–19.
[44] L. Jin, J. Ball, T. Bremner, H.-J. Sue, Crystallization behavior and morphological characterization of poly(ether ether ketone), Polymer 55 (2014) 5255–5265.
[45] B. Wunderlich, Thermal Analysis of Polymeric Materials, Springer, Berlin, 2005.
[46] R. Verma, H. Marand, B. Hsiao, Morphological changes during secondary crystallization and subsequent melting in poly(ether ether ketone) as studied by real time small angle X-ray scattering, Macromolecules 29 (1996) 7767–7775.
[47] C. Fougnies, P. Damman, D. Villers, M. Dosiere, M.H.J. Koch, Time-resolved SAXS, WAXS, and DSC study of the annealing of poly(aryl ether ether ketone) (PEEK) from the glassy state, Macromolecules 30 (1997) 1385–1391.
[48] M. Avrami, Transformation-time relaxtions for random distribution of nuclei, J. Chem. Phys. 8 (1940) 212–224.
[49] F. Rybnikar, Mechanism of secondary crystallization in polymers, J. Polym. Sci. A Gen. Pap. 1 (1963) 2031–2038.
[50] J.E.K. Schawe, Analysis of non-isothermal crystallization during cooling and reorganization during heating of isotactic polypropylene by fast scanning DSC, Thermochim. Acta 603 (2015) 85–93.
[51] J.E.K. Schawe, G.R. Strobl, Superheating effects during the melting of crystallites of syndiotactic polypropylene analysed by temperature-modulated differential scanning calorimetry, Polymer 39 (1998) 3745–3751.
[52] A. Toda, M. Hikosaka, K. Yamada, Superheating of the melting kinetics in polymer crystals: a possible nucleation mechanism, Polymer 43 (2002) 1667–1679.
[53] A. Wurm, M. Merzlyakov, C. Schick, Reversible melting during crystallization of polymers studied by temperature modulated techniques (TMDSC, TMDMA), J. Therm. Anal. Calorim. 60 (2000) 807–820.
[54] A. Wurm, M. Merzlyakov, C. Schick, Crystallization of polymers studied by temperature-modulated techniques (TMDSC, TMDMA), J. Macrom. Sci. Phys. B 38 (1999) 693–708.
[55] J.D. Hoffman, G.T. Davis, J.I. Lauritzen Jr., in: N.B. Hannay (Ed.), Treatise on Solid State Chemistry, vol. 3, Plenum Press, New York, 1976, pp. 497–605. Chap7.
[56] H. Marand, J. Xu, S. Srinivas, Determination of the equilibrium melting temperature of polymer crystals: linear and nonlinear Hoffman-Weeks extrapolations, Macromolecules 31 (1998) 8219–8229.
[57] J. Xu, S. Srinivas, H. Marand, Equilibrium melting temperature and undercooling dependence of the spherulitic growth rate of isotactic polypropylene, Macromolecules 31 (1998) 8230–8242.
[58] H.-L. Chen, R.S. Porter, Melting behavior of poly(ether ether ketone) in its blends with poly(ether imide), J. Polym. Sci. B Polym. Phys. 31 (1993) 1845–1850.
[59] T. Konishi, W. Sakatsuji, K. Fukao, Y. Miyamoto, Temperature dependence of lamellar thickness in isothermally crystallized poly(butylene terephthalate), Macromolecules 49 (2016) 2272–2280.
[60] E. Zhuravlev, J.W.P. Schemlzer, B. Wunderlich, C. Schick, Kinetics of nucleation and crystallization in poly(ε-caprolactone) (PCL), Polymer 52 (2011) 1983–1997.
[61] J. Xu, B. Heck, H.-M. Ye, J. Jiang, Y.-R. Tang, J. Liu, B.-H. Guo, R. Reiter, D.-S. Zhou, G. Reiter, Stabilization of nuclei of lamellar polymer crystals: insights from a comparison of the Hoffman-Weeks line with the crystallization line, Macromolecules 49 (2016) 2206–2215.
[62] A. Gradys, P. Sajkiewics, S. Adamovsky, A. Minakov, C. Schick, Crystallization of poly(vinylidene fluoride) during ultra-fast cooling, Thermochim. Acta 461 (2007) 153–157.
[63] J.D. Hoffman, R.L. Miller, H. Marand, D.B. Roitman, Relationship between the lateral surface free energy σ and the chain structure of melting-crystallized polymers, Macromolecules 25 (1992) 2221–2229.
[64] J.D. Hoffman, R.L. Miller, Kinetics of crystallization from the melt and chain folding in polyethylene fractions revisited; theory and experiment, Polymer 38 (1997) 3151–3212.
[65] P.C. Dawson, D.J. Blundell, X-ray data for poly(aryl ether ketones), Polymer 21 (1980) 577–578.
[66] J.N. Hay, D.J. Kemmish, J.I. Langford, A.I.M. Rae, The structure of crystalline peek, Polym. Commun. 25 (1984) 175–178.